Original article

Deep neural network for automatic volumetric segmentation of whole-body CT images for body composition assessment

Yoon Seong Lee [a, 1], Namki Hong [b, 1], Joseph Nathanael Witanto [c], Ye Ra Choi [d], Junghoan Park [a], Pierre Decazes [e], Florian Eude [e], Chang Oh Kim [f], Hyeon Chang Kim [g], Jin Mo Goo [a, h], Yumie Rhee [b, **], Soon Ho Yoon [a, c, *]

[a] Department of Radiology, Seoul National University College of Medicine, Seoul National University Hospital, Seoul, South Korea
[b] Division of Endocrinology, Department of Internal Medicine, Yonsei University College of Medicine, Seoul, South Korea
[c] MEDICALIP Co. Ltd., Seoul, South Korea
[d] Department of Radiology, Seoul Metropolitan Government-Seoul National University Boramae Medical Center, Seoul, South Korea
[e] Department of Nuclear Medicine, Henri Becquerel Cancer Center, Rouen, France
[f] Division of Geriatrics, Department of Internal Medicine, Severance Hospital, Yonsei University College of Medicine, Seoul, South Korea
[g] Department of Preventive Medicine, Yonsei University College of Medicine, Seoul, South Korea
[h] Institute of Radiation Medicine, Seoul National University Medical Research Center, Seoul, South Korea

A R T I C L E   I N F O

S U M M A R Y

Background & aims: Body composition analysis on CT images is a valuable tool for sarcopenia assessment. We aimed to develop and validate a deep neural network applicable to whole-body CT images of PET-CT scan for the automatic volumetric segmentation of body composition.

Methods: For model development, one hundred whole-body or torso ^{18}F-fluorodeoxyglucose PET–CT scans of 100 patients were retrospectively included. Two radiologists semi-automatically labeled the following seven body components in every CT image slice, providing a total of 46,967 image slices from the 100 scans for training the 3D U-Net (training, 39,268 slices; tuning, 3116 slices; internal validation, 4583 slices): skin, bone, muscle, abdominal visceral fat, subcutaneous fat, internal organs with vessels, and central nervous system. The segmentation accuracy was assessed using reference masks from three external datasets: two Korean centers (4668 and 4796 image slices from 20 CT scans, each) and a French public dataset (3763 image slices from 24 CT scans). The 3D U-Net-driven values were clinically validated using bioelectrical impedance analysis (BIA) and by assessing the model's diagnostic performance for sarcopenia in a community-based elderly cohort (n = 522).

Results: The 3D U-Net achieved accurate body composition segmentation with an average dice similarity coefficient of 96.5%–98.9% for all masks and 92.3%–99.3% for muscle, abdominal visceral fat, and subcutaneous fat in the validation datasets. The 3D U-Net-derived torso volume of skeletal muscle and fat tissue and the average area of those tissues in the waist were correlated with BIA-derived appendicular lean mass (correlation coefficients: 0.71 and 0.72, each) and fat mass (correlation coefficients: 0.95 and 0.93, each). The 3D U-Net-derived average areas of skeletal muscle and fat tissue in the waist were independently associated with sarcopenia (P < .001, each) with adjustment for age and sex, providing an area under the curve of 0.858 (95% CI, 0.815 to 0.901).

---

* Corresponding author. Department of Radiology, Seoul National University College of Medicine, Seoul National University Hospital. 101 Daehak-ro, Chongno-gu, 03080, Seoul, South Korea. Fax: +82 2 743 7418.
** Corresponding author. Department of Internal Medicine, Yonsei University College of Medicine, 50-1 Yonsei-ro, Seodaemun-gu, Seoul 03722, South Korea. Fax: 82 2 393 6884.
E-mail addresses: yumie@yuhs.ac (Y. Rhee), yshoka@gmail.com, Soon.Yoon@umassmed.edu (S.H. Yoon).
[1] Y.S.L. and N.H. contributed equally to this work.

Conclusions: This deep neural network model enabled the automatic volumetric segmentation of body composition on whole-body CT images, potentially expanding adjunctive sarcopenia assessment on PET-CT scan and volumetric assessment of metabolism in whole-body muscle and fat tissues.

1. Introduction

Sarcopenia is a progressive and generalized skeletal muscle disorder involving the loss of muscle volume and function [1]. Sarcopenia is present in 12.9–40.4% of elderly individuals, and is associated with a variety of adverse health outcomes, including falls, functional decline, impaired quality of life, and mortality, especially in combination with obesity [1]. The European Working Group on Sarcopenia in Older People recently updated a practical definition and diagnostic criteria of sarcopenia by including measurements of a combination of muscle mass, strength, and physical performance [2]. Dual-energy X-ray absorptiometry and bioelectrical impedance analysis (BIA) are typically used to assess the mass of appendicular skeletal muscle in the general population [3]. However, the X-ray absorptiometry cannot provide data on skeletal muscle mass in the trunk or muscle adiposity, while BIA cannot measure visceral fat obesity and is prone to various potential sources of error [4].

CT and MRI are widely used cross-sectional imaging modalities in modern medicine and are considered the gold standard for quantifying the amount of muscle and fat in the body [5]. A body composition analysis of a single CT image at the L3 vertebra level can estimate the amount of whole-body muscle and fat [6–8], and this method is widely used to evaluate sarcopenia and visceral obesity [9,10]. Furthermore, a deep-learning algorithm enabled the automatic quantification of muscle and fat amount at the L3 vertebra level, which traditionally required considerable time and resources of experienced readers when segmented manually [11,12].

Nevertheless, the distribution of abdominal muscle and fat differs across levels of the lumbar vertebrae in the waist, implying that the distribution could be fully captured by the volumetric analysis of multiple CT images, rather than a single CT image [11]. If volumetric CT analysis of body composition could be applied to whole-body CT images, it would be possible to assess sarcopenia and visceral obesity on CT images beyond the L3 level (i.e., chest CT) without additional radiation exposure. Particularly, as ^{18}F-fluorodeoxyglucose PET/CT scan is a vital examination for the surveillance of systematic metastasis in cancer patients and covers the whole body [13,14], the volumetric body composition analysis could enable an assessment of whole-body composition at baseline and during follow-up in cancer patients [15,16]. In this study, we aimed to develop and validate a deep neural network for the volumetric segmentation of body composition applicable to whole-body CT images of PET-CT scan.

2. Materials and methods

The institutional review board of the participating institutions approved this retrospective study for model development, and the requirement for informed patient consent was waived. Analysis of the Korean Urban Rural Elderly (KURE) cohort was approved by the institutional review board after obtaining written consent from all participants prior to the study.

2.1. Study population

For the training dataset, we retrospectively collected 100 unenhanced whole-body CT scans of PET/CT examination (46,967 CT image slices in total; 145 to 992 image slices per CT scan) from 100 patients, preferentially for the purpose of an initial staging workup of early lung cancer or systematic screening at a single
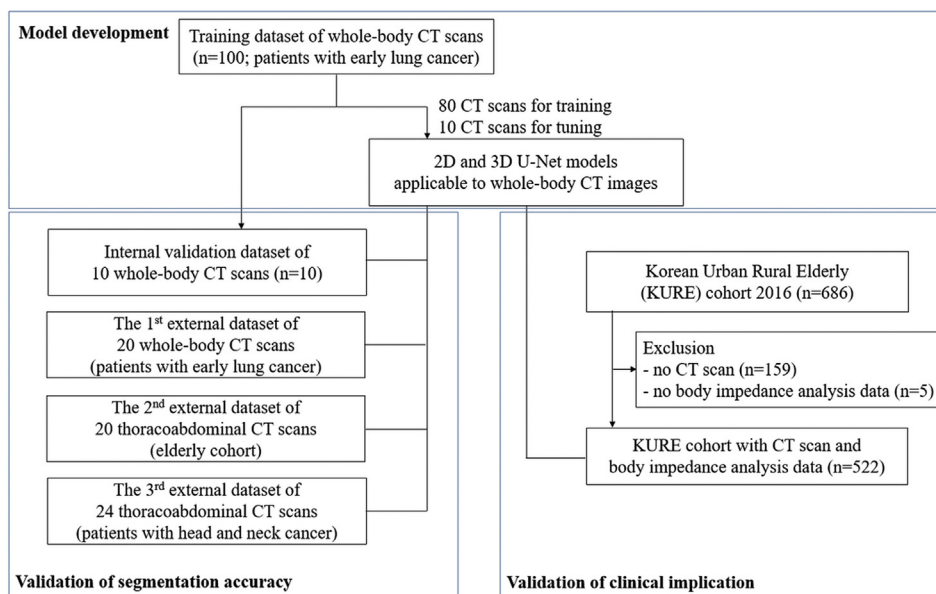

Fig. 1. Study diagram for model development and validation.

Table 1
Composition of the internal and external datasets for model development and validation.

	Internal dataset	External validation datasets			
		The first dataset	The second dataset	The third dataset	The fourth dataset
Purpose	Model development	Assessing segmentation accuracy			Clinical validation
Country	Korea	Korea	Korea	France	Korea
Number of patients	100	20	20	18	522
Number of CT scans	100	20	20	24	522
Age (years)	62.3 ± 13.3	68.0 ± 10.5	74.0 ± 3.7	58.5 ± 9.3	75.3 ± 4.5
Sex (male:female)	40:60	11:9	9:11	15:3	170:352
Body mass index	23.1 ± 3.9 (13.8—31.2)	23.4 ± 2.5 (17.9—26.4)	23.5 ± 2.6 (16.4—29.4)	Unknown	24.4 ± 3.2 (14.9—36.9)
CT Vendors	Siemens Healthineers; Philips Medical Systems	Philips Medical Systems	Siemens Healthineers	GE Healthcare	Siemens Healthineers
CT machines	mBiograph40, mBiograph64; GEMINI	GENIMI TF TOF 64	SOMATOM Definition AS+	Discovery ST, HR, RX, and STE	SOMATOM Definition AS+
CT scan range	Head, neck, torso, and arm, 64; Whole body, 36	Head, neck, torso, and arm	Torso	Torso	Torso
CT slice thickness	2—6.5 mm	4 mm	3 mm	5 mm	3 mm
CT slices per scan	145—992	213—255	200—269	117—232	239—268
Tube voltage (kVp)	100—120	120	100	120	100
Tube current (Ref mAs)	40—67	50	200	300	200

Abbreviation: CT, computed tomography; kVp, peak kilovoltage; Ref mAs, Reference milliampere-second. Data in the parenthesis indicates the range of body mass index. All CT scans were obtained without contrast enhancement.

tertiary center (Fig. 1). We used three datasets from other institutions for external validation to evaluate segmentation performance between the reference masks and the network-derived masks (Table 1): the first dataset contained 20 CT scans (4668 CT image slices in total; 213 to 255 image slices per CT scan) of 20 patients with stage I lung cancer, the second dataset contained 20 CT scans (4796 CT image slices in total; 200 to 269 image slices per CT scan) of 20 participants in a community-based older adult cohort with 20 CT scans, and the third dataset contained 24 CT scans (3763 CT image slices in total, 117 to 232 image slices per CT scan) of 18 patients with head and neck cancer. For clinical validation, we used the KURE cohort as a fourth external dataset [17]. Details about the validation datasets are summarized in Table 1.

2.2. Preparation of training CT data

All the whole-body CT images were processed in a commercially available software program (MEDIP PRO v2.0.0.0, MEDICALIP Co. Ltd., Seoul, Korea) for semi-automatic segmentation of the following seven components of body composition: skin, bone, muscle, abdominal visceral fat (AVF), subcutaneous fat (SF), internal organs and vessels (IO), and central nervous system (CNS). The bone mask extended from the skull to the phalanges and contained the hyoid bone, cricoid, arytenoid, thyroid cartilages, and rib cartilages. The muscle mask included skeletal muscles, including the proximal portion of the thin diaphragm and crus as much as recognizable, resulting in the exclusion of the central tendon of the diaphragm. The AVF mask included fatty tissues of peritoneal and retroperitoneal spaces [18] that were distributed below the xiphoid process and diaphragmatic hiatus to the perirectal fat. In the SF mask, we did not separate SF from intramuscular fat and intrathoracic visceral fat and combined those fatty tissues. The IO mask contained intraabdominal and intrathoracic solid organs, hollow viscera, breast tissue, external genital organs, and the thyroid gland, along with the major arteries and veins. The distal ends of separation between muscle and vessels were the upper end of the thyroid superiorly, the proximal biceps brachii laterally, and the upper one-third of the femur inferiorly. The vessels beyond the distal ends were included in the muscle mask. We excluded parotid glands from any of the masks while including salivary and submandibular glands in the muscle mask, as the latter two glands could not be separated from muscle on noncontrast CT images. The CNS mask comprised the eyeball, intracranial structures, and the spinal canal.

Table 2
Dice similarity coefficients, sensitivity, and precision between the reference masks and 3D-UNet-derived masks in internal and external validation datasets.

	Skin			Bone			Muscle			Abdominal visceral fat		
	DSC	Sens	PPV	DSC	Sens	PPV	DSC	Sens	PPV	DSC	Sens	PPV
2D U-Net												
Internal dataset	92.2 ± 5.6	90.4 ± 9.3	94.5 ± 3.2	97.6 ± 2.1	96.8 ± 3.8	98.6 ± 0.4	97.2 ± 1.0	97.6 ± 0.9	96.9 ± 1.4	90.5 ± 7.8	87.1 ± 11.5	94.9 ± 5.0
External dataset 1	80.7 ± 0.8	84.0 ± 1.0	77.6 ± 1.6	96.3 ± 0.5	95.3 ± 0.7	97.3 ± 0.5	95.7 ± 0.7	95.4 ± 0.9	95.9 ± 0.6	93.1 ± 3.6	91.7 ± 5.0	94.6 ± 2.2
External dataset 2	93.9 ± 1.8	93.8 ± 1.0	94.1 ± 3.1	97.7 ± 0.6	96.6 ± 0.9	98.8 ± 0.4	97.0 ± 0.8	96.7 ± 1.4	97.3 ± 0.8	94.2 ± 3.5	94.1 ± 4.0	94.2 ± 3.1
External dataset 3							89.9 ± 2.2	86.9 ± 2.3	93.2 ± 3.1	88.3 ± 8.2	87.3 ± 11.7	90.0 ± 3.9
3D U-Net												
Internal dataset	94.0 ± 4.5	92.6 ± 7.3	95.9 ± 3.8	98.1 ± 2.0	98.2 ± 3.0	98.0 ± 1.0	98.1 ± 0.6	98.5 ± 0.8	97.8 ± 0.7	95.1 ± 4.9	94.3 ± 7.5	96.0 ± 2.5
External dataset 1	95.4 ± 0.8	94.5 ± 1.0	96.3 ± 0.9	98.2 ± 0.5	98.8 ± 0.5	97.5 ± 0.8	96.8 ± 1.3	96.0 ± 2.2	97.5 ± 0.5	96.3 ± 2.2	97.0 ± 1.4	95.7 ± 3.6
External dataset 2	98.6 ± 1.1	98.0 ± 1.5	99.3 ± 0.7	99.4 ± 0.5	99.7 ± 0.3	99.1 ± 0.8	99.2 ± 0.5	99.5 ± 0.5	99.0 ± 0.6	98.9 ± 1.4	99.1 ± 0.9	98.7 ± 2.1
External dataset 3							90.3 ± 1.7	86.8 ± 2.0	94.1 ± 2.8	92.4 ± 4.7	91.8 ± 6.8	93.2 ± 3.0

Abbreviation: DSC = dice similarity coefficient; Sens = sensitivity; PPV = positive predictive value.
Data in columns indicate percentages of mean ± standard deviation. The third external dataset, French public dataset, only contained masks for muscle, abdominal visceral, and subcutaneous fat tissues.

A technician and one radiology resident (Y.S.L. with 3 years of body CT interpretation) initially segmented the CT images by using thresholds of Hounsfield units (HU), providing rough masks of muscle, fat, and bone as follows: -29 to 150 HU for skeletal muscle, -190 to -30 HU for adipose tissue, >250 HU for bone. Then, one body radiologist (S.H.Y., with 15 years of body CT interpretation) checked and adjusted the masks in 46,967 axial CT image slices from 100 CT scans for the training dataset by manual correction, morphological closing, subtraction, and merging. Two body radiologists (J.H.H. and J.H.P. with 6 and 5 years of body CT interpretation, each) prepared the reference masks for the first and second external validation data of the 20 CT scans in a similar way, respectively. Reference masks in the third external validation data were prepared by the French nuclear medicine physician (P.D. with 8 years of experience in PET/CT scan).

2.3. Development and materialization of the deep neural network

The 100 CT scans were randomly assigned into one of the three following data sets: 80 cases (39,268 CT image slices) for the training set, 10 cases (3116 CT image slices) for the tuning set, and 10 cases (4583 CT image slices) for the internal validation set. Most of the CT scans consisted of 2-mm-section CT images that covered the head to the lower arm and mid-thigh. The training data of CT images were normalized using the soft tissue window setting.

We trained two-dimensional (2D) and three-dimensional (3D) U-Nets for segmentation [19,20]. The 2D U-Net used 2D convolutional kernels to segment anatomic structures for a single axial image slice and conducted the segmentation of multiple CT images by serially segmenting one image slice at a time, while not considering information about adjacent cephalocaudal CT image slices. The 3D U-Net used 3D convolutional kernels for the same task and segmented a series of cephalocaudal axial CT image slices at a time as a volumetric patch to conduct the segmentation.

The 2D U-Net received an input size of $512 \times 512 \times 1$ and consisted of initial convolutions, four encoders, four decoders, and a final convolution. Except for the final convolution (a 1×1 convolution), every convolutional layer consisted of a 3×3 convolution followed by batch normalization [21] and the rectified linear unit activation function [22]. For decoders, up-sampling with the bilinear interpolation method was used, followed by concatenation to conserve information before down-sampling. The 3D U-Net received an input size of $512 \times 512 \times 8$ and used three encoders and three decoders. Except for the final convolution (a $1 \times 1 \times 1$ convolution), every convolutional layer consisted of a $3 \times 3 \times 3$ convolution, followed by ReLU and group normalization. The first encoder adopted $1 \times 2 \times 2$ max pooling to preserve data in the z-axis, whereas the second and third encoders used $2 \times 2 \times 2$ max pooling. For decoders, up-sampling with tri-linear interpolation was used. The Kaiming He initialization method [23] was used for weight initialization. Both models used a softmax function at the final layer and were trained using the stochastic gradient descent algorithm and cross-entropy loss function.

The 2D and 3D U-Net models were packaged as a standalone software (DeepCatch v1.0.0.0; http://www.medicalip.com/Download) by a functional modification of the FDA-approved MEDIP PRO v2.0.0.0. The specifications required for running the U-Net models are as follows: operating system, Microsoft Windows 7 (64 bit; IBM Corporation, San Jose, CA) or higher; central processing unit, Intel i5 (Intel Corporation, Santa Clara, CA) or higher; random-access memory, 8 GB or higher; and graphics processing unit, GeForce 1000 series or higher (NVIDIA Corporation, Santa Clara, CA) with the minimum memory of 2 GB or larger for 2D U-Net and 8 GB or larger for 3D-UNet supporting the Compute Unified Device Architecture with the latest drivers. In the external validation datasets that each CT scan consisted of about two hundred CT image slices, the segmentation per CT scan was accomplished in around 45 s for the 2D U-Net model and in around 75 s for the 3D U-Net model with the recommended specifications.

2.4. Clinical validation cohort: KURE

The KURE cohort is a government-funded cohort of community-based Korean older adults, in whom cardiovascular, musculoskeletal, and age-related diseases were studied [17]. A total of 3517 subjects participated in the study between 2012 and 2015, and a follow-up study was completed between 2016 and 2019 (n = 2520). CT images of the torso area (from neck to mid-thigh level) were obtained in the follow-up study through a comprehensive assessment of musculoskeletal function, physical performance, and radiological and biochemical measurements. Because CT images were only available at follow-up, a subset of the data of the KURE cohort collected in 2016 was analyzed using the 3D U-Net driven model as the clinical validation set (n = 522). Details of the KURE cohort can be obtained in the cohort profile [24]. The KURE population was included in prior studies on study protocol [17,24], vitamin D [25–27], dysmotility [28], and metabolic syndrome [29,30].

All CT scans in KURE participants were performed using SOMATOM Definition CT scanner (Siemens Healthcare, Germany) according to a predefined cohort protocol (noncontrast CT, slice thickness 3 mm, tube voltage 100 kV, tube current 200 mA, reconstruction with standard kernel) [17,24].

Skin	Abdominal visceral fat	Subcutaneous fat			Internal organs and vessels			Central nervous system		
PPV	PPV	DSC	Sens	PPV	DSC	Sens	PPV	DSC	Sens	PPV
2D U-Net										
94.5 ± 3.2	94.9 ± 5.0	96.1 ± 3.1	96.7 ± 3.7	95.5 ± 3.0	96.3 ± 1.3	96.3 ± 1.4	96.3 ± 1.4	97.5 ± 3.3	97.1 ± 3.7	98.0 ± 3.1
77.6 ± 1.6	94.6 ± 2.2	94.3 ± 2.5	94.7 ± 3.1	94.0 ± 2.1	94.5 ± 0.8	94.5 ± 1.1	94.4 ± 1.6	98.4 ± 0.2	98.5 ± 0.4	98.5 ± 0.3
94.1 ± 3.1	94.2 ± 3.1	97.4 ± 0.8	99.4 ± 0.3	95.4 ± 1.3	96.0 ± 1.5	95.7 ± 1.0	96.4 ± 2.3	92.8 ± 2.8	90.7 ± 4.6	95.2 ± 2.9
	90.0 ± 3.9	92.7 ± 2.9	97.3 ± 0.8	88.5 ± 4.9						
3D U-Net										
95.9 ± 3.8	96.0 ± 2.5	97.1 ± 3.1	96.2 ± 4.2	98.0 ± 2.0	97.6 ± 0.8	97.4 ± 0.7	97.8 ± 1.3	98.0 ± 2.9	97.9 ± 3.4	98.2 ± 3.0
96.3 ± 0.9	95.7 ± 3.6	98.0 ± 1.0	97.8 ± 1.1	98.2 ± 1.0	94.2 ± 2.5	96.1 ± 1.2	92.5 ± 4.1	96.8 ± 2.0	98.5 ± 0.3	95.2 ± 3.8
99.3 ± 0.7	98.7 ± 2.1	99.7 ± 0.3	99.6 ± 0.4	99.7 ± 0.3	98.7 ± 0.8	98.4 ± 0.8	99.0 ± 1.1	98.4 ± 2.0	97.2 ± 3.6	99.7 ± 0.5
	93.2 ± 3.0	94.1 ± 2.5	96.8 ± 0.9	91.6 ± 4.2						

2.5. Definition of sarcopenia and dysmobility syndrome

Sarcopenia was defined based on Asian Working Group for Sarcopenia 2019 consensus statement as low appendicular lean mass with low muscle strength or low physical performance [24,31]. Appendicular lean mass was assessed using multi-frequency segmental bioimpedance analysis (InBody720, Biospace, Seoul, Korea; appendicular lean mass/height^2 < 7.0 kg/m^2 in men; < 5.7 kg/m^2 in women). Low muscle strength was defined as maximum handgrip strength <28 kg in men or <18 kg in women. Low physical performance was measured by the five-time chair stand test (12 s or higher). Dysmobility syndrome was defined as having at least three of the following factors using modified definitions: falls in the preceding year, low grip strength (<28 kg in men or < 18 kg in women), low bone mass (quantitative computed tomography-based volumetric trabecular bone mineral density in the lumbar spine < 80 mg/mm^3) [32], low appendicular lean mass (appendicular lean mass/height^2 < 7.0 kg/m^2 in men; < 5.7 kg/m^2 in women), high fat mass (>30% in men; > 40% in women), and low performance on the timed get-up-and-go test (12 s or higher) [33,34].

2.6. Statistical analysis

In the development cohorts, we compared the reference masks obtained through semi-automatic segmentation with U-Net-drive masks using the Dice similarity coefficient (DSC), sensitivity, and positive predictive value (PPV) [35]. The DSC provided the degree of segmentation similarity between U-Net-driven and reference masks. The sensitivity measured the portion of voxels in the reference mask that were also included in the U-Net mask. PPV measured the ratio of pixels in the U-Net-driven mask that was correctly present in the reference mask (Fig. S1). The paired t-test was used to compare the segmentation performance between the 2D and 3D U-Net. The independent t-test was used to compare segmentation performance depending upon sex, age (≤70 years vs. >70 years), body mass index (BMI) (≤23 kg/m^2 vs. >23 kg/m^2), and CT scan range (T12 or above vs. below T12).

In the clinical validation cohort, we calculated the 3D U-Net-driven torso volume of skeletal muscle and fat tissue (cm^3; representative of near whole-body volume composition except for appendicular body parts) and the average areas of skeletal muscle and fat tissue in the 3D U-Net-driven waist volume (cm^2; representative of single CT slice body composition in the waist): The latter were presented as average skeletal muscle area (SMA, cm^2) and body fat area (BFA, cm^2) by dividing the volume of those tissues in the waist by the craniocaudal length of the waist. The waist ranges from the lower margin of the last rib to the upper margin of iliac crest [36], containing the L3 vertebra [37]. The average SMA and BFA represented the mean distribution of SMA and BFA in the waist and could be used equivalently to single-slice measures at L3 [2]. Skeletal muscle index (SMI, cm^2/m^2) and body fat index (BFI, cm^2/kg) were also calculated by dividing SMA and BFA by height squared and kilograms, respectively. We assessed the correlation between 3D U-Net-driven CT parameters and BIA-based values. Linear regression models were used to estimate the cutoffs of 3D U-Net-derived SMI and BFI that corresponded to the currently endorsed BIA-based diagnostic thresholds for sarcopenia or dysmobility syndrome (low appendicular lean mass [appendicular lean mass/height^2 <7.0 kg/m^2 in men; <5.4 kg/m^2 in women] and high fat mass [body fat percent >30% in men; >40% in women]) [31,33,34,38]. Multivariable logistic regression models were used to evaluate the 3D U-Net-driven average SMA and BFA in the waist with sarcopenia and dysmobility syndrome as a continuous or

binary variable based on the cutoffs while adjusting for covariates. We compared the area under the receiver operating characteristic curve (AUROC) to evaluate whether the 3D U-Net-derived average SMA and BFA in the waist could improve diagnostic performance when added to age and sex [39]. All analyses were performed using STATA version 14.1 (StataCorp, College Station, TX, USA). The statistical significance level was set at a two-sided P-value of <0.05.

3. Results

3.1. Segmentation performance in the development set

The mean age and sex distribution of the subjects in the development set (internal set) and the three external validation sets for segmentation accuracy were 62.3 ± 13.3 years (women, 60%), 68.0 ± 10.5 years (women, 45%), 74.0 ± 3.7 years (women, 55%), and 58.5 ± 9.3 years (women, 17%), respectively (Table 1). Both the 2D and 3D U-Net achieved accurate body composition segmentation (Table 2 and Fig. 2), and the 3D U-Net performed significantly better than the 2D U-Net for all seven masks (Table S1). The average DSCs between the U-Net results and the reference for all masks were as follows: the internal dataset, 95.3 ± 3.0% and 96.9 ± 2.4%, each; the first external dataset, 93.3 ± 1.0% and 96.5 ± 1.1%, each; and the second external dataset, 95.6 ± 1.1% and 98.9 ± 0.4%, each. When confined to muscle, AVF, and SF masks, the average DSCs between the 2D and 3D U-Net results and the reference masks were as follows: the internal dataset, 94.6 ± 5.6% and 96.8 ± 3.5%, each; the first external dataset, 94.4 ± 2.7% and 97.0 ± 0.9%, each; the second validation dataset, 96.2 ± 2.5% and 99.3 ± 0.9%, each; the third external dataset, 90.3 ± 3.6% and 92.3 ± 2.2%, each. The segmentation performance of the 3D U-Net was generally not affected by age, sex, BMI, or scan range (Table S2).

3.2. Correlation between 3D U-Net parameters and BIA

In the KURE cohort, the Pearson correlation coefficients between the 3D U-Net-driven CT skeletal muscle measurements and BIA-based appendicular lean mass values ranged from 0.59 to 0.72 and from 0.56 to 0.66 in men and women, respectively (Table 3). Body fat mass and percent measured by BIA showed excellent correlations with CT-based torso fat volume and waist BFA in both men and women (correlation coefficient, 0.82 to 0.95; P < .001 for all).

The average SMI values of the waist of 40 cm^2/m^2 (men) and 35 cm^2/m^2 (women) corresponded to the BIA-based clinical thresholds for low appendicular lean mass (7.0 kg/m^2 in men and 5.7 kg/m^2 in women) in the linear regression model (Fig. 3). The BFI values of the waist of 4.7 cm^2/kg (men) and 5.8 cm^2/kg (women) corresponded to the BIA-based high fat mass thresholds (30% in men and 40% in women), respectively (see Fig. 3).

3.3. Associations of 3D U-Net body composition assessments with sarcopenia

In the KURE cohort, which was used for clinical validation, study participants with sarcopenia defined using low BIA-derived ALM with low muscle strength or low physical performance according to AWGS 2019 consensus (n = 85, 16%) had older age, lower BMI, and higher prevalence of low handgrip strength, low lean mass, and low physical performance measured by the timed get-up-and-go test or the five-time chair rise test compared to those without sarcopenia (Table S3, P < .05 for all). Individuals with dysmobility syndrome (n = 149, 29%) showed similar results
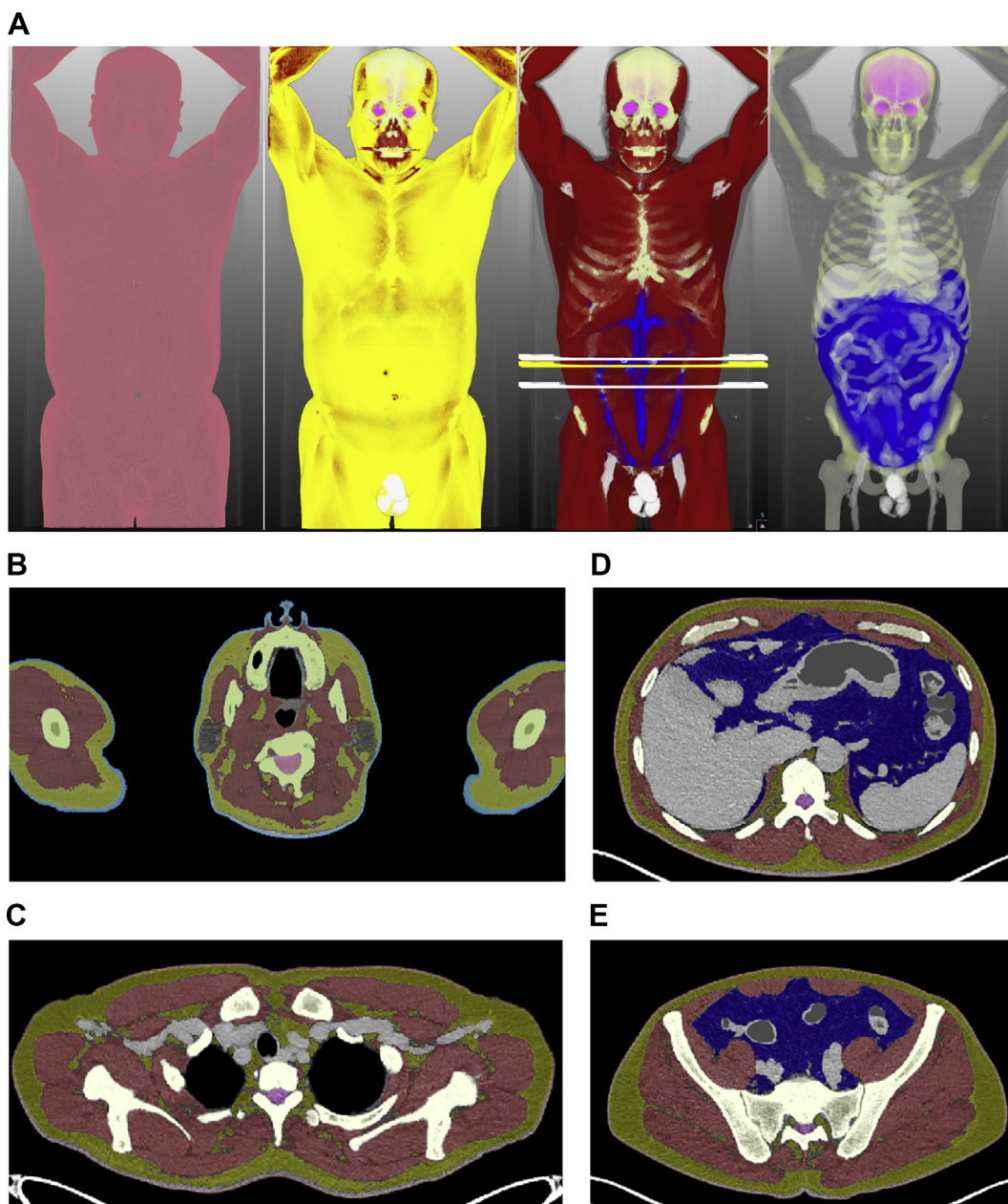
Fig. 2. Representative 3D reformatted (A) and cross-sectional (B–E) CT images of 3D U-Net-derived masks in a 67-year-old male patient who underwent surgical resection of early lung cancer (body mass index, 27.0 kg/m^2). (A) The four images sequentially show skin, subcutaneous fat, muscle, and abdominal visceral fat, along with bone, internal organs and vessels, and the central nervous system. Overlaid lines indicate the waist (white lines), and the L3 level (yellow line). (B–E) The images show cross-sectional areas of head and upper arm (B), thoracic inlet (C), upper abdomen (D), and pelvis (E). Note that the parotid glands are excluded from any masks as intended (A), and the borders of axillary vessels (B), outer margins of liver and spleen (C), and common iliac vessels (D) are well separated from adjacent muscles. The average Dice similarity coefficient for the seven classes was 98.2%, and the Dice similarity coefficients for each class were as follows: skin (pink), 95.7%; subcutaneous fat (yellow), 98.2%; skeletal muscle (brown), 98.4%; abdominal visceral fat (blue), 98.6%; bone (light beige), 98.8%; internal organs and vessels (light gray), 97.6%; and central nervous system (light pink), 99.1%. . (For interpretation of the references to color in this figure legend, the reader is referred to the Web version of this article.)

Table 3
Correlations between 3D U-Net-derived CT parameters and BIA values for body composition assessment.

Comparator (3D U-Net-driven CT parameters)	Reference (BIA)	Men (n = 170)		Women (n = 352)	
		Correlation coefficients	P-value	Correlation coefficients	P-value
Torso skeletal muscle volume (cm^3)	ALM (kg)	0.71	<0.001	0.66	<0.001
Average skeletal muscle area in the waist (cm^2)	ALM (kg)	0.72	<0.001	0.65	<0.001
Torso skeletal muscle index (cm^3/m^2)	ALMI (kg/m^2)	0.59	<0.001	0.56	<0.001
Average skeletal muscle index in the waist (cm^2/m^2)	ALMI (kg/m^2)	0.60	<0.001	0.58	<0.001
Torso fat volume (cm^3)	Fat mass (kg)	0.95	<0.001	0.94	<0.001
Average fat area in the waist (cm^2)	Fat mass (kg)	0.93	<0.001	0.92	<0.001
Torso body fat index (cm^3/kg)	Body fat percent (%)	0.90	<0.001	0.86	<0.001
Average body fat index in the waist (cm^2/kg)	Body fat percent (%)	0.86	<0.001	0.82	<0.001

Abbreviation: BIA, body impedance analysis; ALMI, appendicular lean mass index.
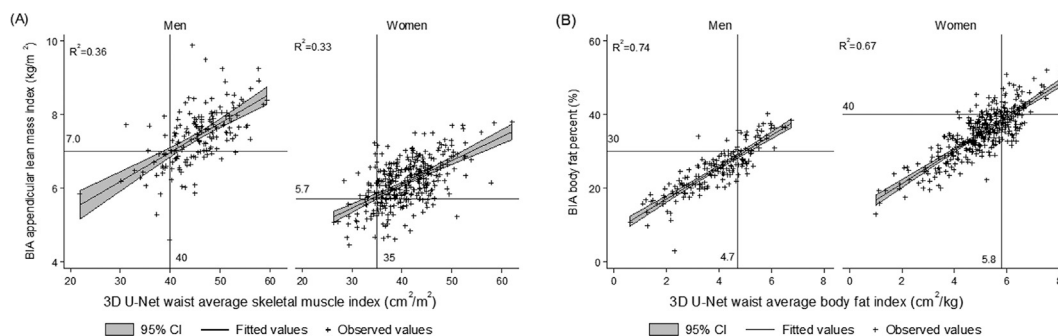
Fig. 3. Estimated cutoffs of computed tomographic average skeletal muscle index and body fat index in the waist. Cutoffs of 40 cm²/m² and 35 cm²/m² in men and women, respectively, in the average skeletal muscle index of the waist corresponded to bioelectrical impedance analysis-based clinical thresholds for low appendicular lean mass (7.0 kg/m² in men and 5.7 kg/m² in women) in the linear regression model. Cutoffs of 4.7 cm²/kg and 5.8 cm²/kg in men and women, respectively, in the average body fat index of the waist corresponded to bioelectrical impedance analysis-based high fat mass thresholds (30% in men and 40% in women).
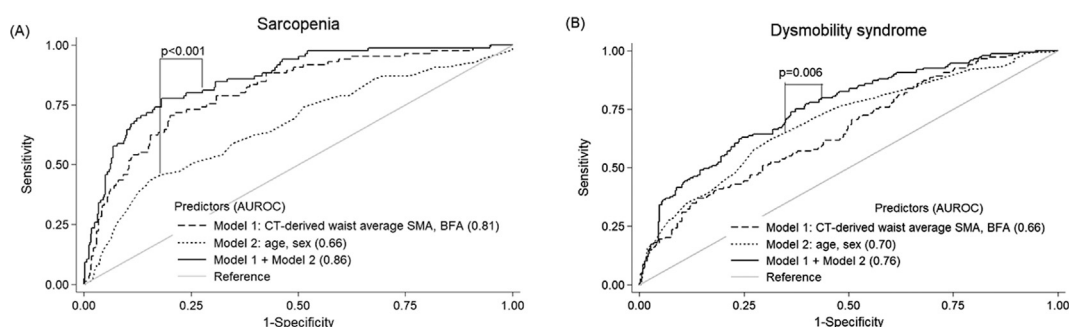

Fig. 4. Improved diagnostic performance for sarcopenia and dysmobility syndrome achieved by adding average skeletal muscle area (SMA) and body fat area (BFA) in the waist to age and sex. The average SMA and BFA in the waist showed a modest to good discriminatory performance for sarcopenia (AUROC 0.81, 95% CI 0.75 to 0.85) or dysmobility syndrome (AUROC 0.66, 95% CI 0.60 to 0.70). Adding the average SMA and BFA to age- and sex-based models significantly improved the diagnostic performance for sarcopenia (AUROC 0.66 versus 0.81; p < .001) and dysmobility syndrome (AUROC, 0.70 versus 0.76; P = .006).

Table 4
Logistic regression analyses for sarcopenia and dysmobility syndrome.

	Univariate model		Multivariable model 1		Multivariable model 2	
	OR (95% CI)	P-value	OR (95% CI)	P-value	OR (95% CI)	P-value
Sarcopenia						
Average SMA in the waist, per 1 sd decrease[a]	2.46 (1.80–3.35)	<0.001	4.03 (2.55–6.36)	<0.001	–	–
Average BFA in the waist, per 1 sd increase+	0.39 (0.30–0.51)	<0.001	0.51 (0.38–0.69)	<0.001	–	–
Low average SMI in the waist (vs. high)[b]	5.67 (3.30–9.76)	<0.001	–	–	5.35 (3.03–9.46)	<0.001
High average BFI in the waist (vs. low)[b]	0.40 (0.21–0.75)	0.004	–	–	0.43 (0.22–0.84)	0.013
Age, per 1 year increase	1.13 (1.08–1.19)	<0.001	1.10 (1.04–1.17)	0.001	1.14 (1.08–1.20)	<0.001
Women (vs. men)	0.72 (0.44–1.16)	0.180	0.17 (0.07–0.39)	<0.001	0.88 (0.51–1.50)	0.644
Dysmobility syndrome						
Average SMA in the waist, per 1 sd decrease[a]	1.81 (1.45–2.26)	<0.001	3.47 (1.99–6.04)	<0.001	–	–
Average BFA in the waist, per 1 sd increase+	1.05 (0.88–1.25)	0.573	2.33 (1.48–3.67)	<0.001	–	–
Low average SMI in the waist (vs. high)[b]	2.81 (1.70–4.65)	<0.001	–	–	3.48 (1.99–6.04)	<0.001
High average BFI in the waist (vs. low)[b]	1.81 (1.21–2.72)	0.004	–	–	2.34 (1.49–3.67)	<0.001
Age, per 1 year increase	1.15 (1.10–1.21)	<0.001	1.18 (1.12–1.24)	<0.001	1.19 (1.12–1.25)	<0.001
Women (vs. men)	1.60 (1.05–2.45)	0.030	2.56 (1.58–4.16)	<0.001	2.57 (1.58–4.16)	<0.001

Abbreviation: SMA, skeletal muscle area (cm²); BFA, body fat area (cm²); SMI, skeletal muscle index (cm²/m²); BFI, body fat index (cm²/kg).
[a] 1sd = 20 cm²; +1sd = 100 cm².
[b] CT body composition parameters were entered into models separately as continuous variables (average SMA and BFA in the waist) or as categorical variables (Low average SMI or high average BFI in the waist). 40 cm²/m² and 35 cm²/m² in men and women were used for defining the low average SMI, and 4.7 cm²/kg and 5.8 cm²/kg in men and women were used for the high average BFI.

to those of subjects with sarcopenia. However, they had a higher prevalence of high fat mass than those without dysmobility syndrome. Compared to subjects without sarcopenia, individuals with sarcopenia had lower 3D U-Net based CT torso volumetric SMI (3348 vs. 3826 cm³/m²), waist areal SMI (38 vs. 43 cm²/m²), torso volumetric BFI (197 vs. 233 cm³/kg), and waist areal BFI (4.0 vs. 4.8 cm²/kg; P < .001 for all).

3.4. Diagnostic value of 3D U-Net assessments for sarcopenia and dysmobility syndrome

A low average SMI in the waist using the cutoffs of 40 cm²/m² in men and 35 cm²/m² in women alone showed 82% and 71% agreement with a clinical diagnosis of sarcopenia (sensitivity, 38%; specificity, 90%; PPV, 43%; negative predictive value, 88%) and

dysmobility syndrome (sensitivity, 24%; specificity, 90%; PPV, 49%; negative predictive value, 75%), respectively.

A one-standard deviation decrease of the average SMA and BFA in the waist (cm^2) was associated with 2.46- and 1.81-fold elevated odds for sarcopenia and dysmobility syndrome, respectively ($P < .001$ for all) (Table 4). Low average SMI (cm^2/m^2) and high BFI (cm^2/kg) in the waist according to the cutoffs were independently associated with sarcopenia (low SMI, adjusted odds ratio [aOR] 5.35; high BFI, aOR 0.51) and dysmobility syndrome (low SMI, aOR 3.48; high BFI, aOR 2.34; $P < .05$ for all) after adjusting for age and sex. In receiver operating characteristic curves (Fig. 4), the average SMA and BFA in the waist provided an AUROC of 0.81 (95% CI 0.75 to 0.85) for sarcopenia and an AUROC of 0.66 (95% CI 0.60 to 0.70) for dysmobility syndrome. The average SMA and BFA in the waist improved diagnostic performance for sarcopenia (AUROC 0.66 to 0.86, $P < .001$) and dysmobility syndrome (AUROC 0.70 to 0.76, $P = .006$) when added to age and sex.

4. Discussion

The 2D and 3D U-Nets developed in this study were validated in several datasets, including the three of the four major clinical CT vendors [40]. The correlations observed between the U-Nets and the reference values in the internal validation dataset were relatively well reproduced in the external validation datasets. The 3D U-Net performed better than the 2D U-Net for all masks, and the performance of the 3D U-Net was mostly maintained regardless of age, sex, BMI, and scan range. The magnitude of the correlations was slightly lower in the French public dataset than in the other two external validation datasets. This partly originated from differences in the individual standards for muscle (i.e., whether they contained axillary vessels) and AVF (i.e., whether some feces and outer boundaries outside the pelvic floor muscle were contained) in the French public dataset.

Sarcopenia has long been considered a disease of the elderly. However, recent studies suggest that sarcopenia begins earlier in life [41], underscoring the importance of early detection and intervention. Nevertheless, the sarcopenia or preclinical stage of sarcopenia is under-detected, as clinical suspicion for sarcopenia merely initiates the current diagnostic approach of sarcopenia. More than 100 million diagnostic CT examinations of various body parts are performed annually in the world, and early detection of sarcopenia could be improved if sarcopenia is adjunctively evaluated using diagnostic CT scans with a deep neural network for body composition analysis [42]. Indeed, our deep neural network showed excellent correlations with the results of BIA, and provided a diagnostic accuracy of 0.86 for sarcopenia when combined with age and sex.

The seven classes contained all body areas except for the lung and airway that are segmentable using pre-existing mathematical or deep learning approaches [43]. A skin mask can be used to directly measure body surface area [44] or various body circumference values [45] on CT images. The body surface area is crucial for determining the dosage of chemotherapeutic drugs and assessing renal clearance or the cardiac index. The area is generally estimated well by various formulae, but the estimation is less accurate in underweight or overweight individuals and children [46], who potentially benefit from direct measurements. A bone mask can allow a volumetric assessment of bone mineral density in multiple bones simultaneously. IO and CNS masks can serve as input data that accelerate the development of deep neural networks for segmenting particular organs or intra-organ abnormalities.

Our study has several limitations. First, the amount of validation data for assessing the DSC was relatively small, which was somewhat inevitable as the required time and resources for preparing the reference dataset were substantial. Second, our

datasets preferentially included the elderly population. The elderly population typically has lower muscle volume and quality and more abundant fatty tissue than young population. Although the distribution of BMI in the datasets broadly covered underweight to obese patients, the segmentation performance of U-Net might not be sufficiently validated in the young population. Third, the muscle mask inevitably contained distal peripheral vessels, and intrathoracic visceral fat and intramuscular fat were included in the SF mask. Fourth, we only validated the U-Net-driven muscle and fat volume in the abdominal area in the elderly cohort, although the network was applicable to other body parts (e.g., thoracic area). Fifth, we only presented the results of the U-Net models for noncontrast CT scan due to difficulty in preparing a sufficient number of reference data, while the 3D U-Net for contrast CT scan was also developed. The 3D U-Net showed a similar DSC of 95.4% for all masks (muscle, 96.7%, AVF, 95.1%; SF, 96.2%) in the preliminary analysis of the internal dataset. Vessels and organs have varying CT attenuations according to intravascular contrast administration, affecting the segmentation accuracy of U-Net models: soft tissue CT attenuation in noncontrast CT scans (potentially misrecognized as muscles) and high CT attenuation in contrast-enhanced CT scans (potentially misrecognized as bony structures). The separate development of U-Net models for noncontrast and contrast CT scans could provide a robust segmentation for body composition regardless of contrast enhancement. Sixth, the training dataset lacked any patients with ascites, major anatomical variations, or diffuse subcutaneous edema; therefore, it is uncertain whether this algorithm will also work well in such cases.

5. Conclusion

A deep neural network enabled the automatic volumetric segmentation of body composition on whole-body CT images, and the 3D U-Net-derived average areas of skeletal muscle and fatty tissue in the waist were independently associated with sarcopenia and dysmobility syndrome in the elderly. The network-driven automatic volumetric segmentation of CT images of PET-CT scan will enable body composition analysis as adjunctive output of PET-CT scan and volumetric analysis of metabolism in whole-body fat and muscle.

Author contributions

Conceptualization, Y.S.L., N.H., Y.R., S.H.Y., J.M.G.; Data curation, Y.S.L., Y.R.C., J.P., P.D., E.F., C.O.K., H.C.K., Y.R., S.H.Y.; Formal analysis, Y.S.L., N.H., Y.R., S.H.Y.; Investigation, Y.S.L., N.H., Y.R., S.H.Y.; Methodology, Y.S.L., N.H., Y.R., S.H.Y.; Project administration, N.H., Y.R., S.H.Y.; Resources, N.H., Y.R., S.H.Y.; Software, J.N.W.; Supervision, Y.R., S.H.Y.; Validation. Y.R.C., J.P., P.D., E.F., N.H., Y.R., S.H.Y. Visualization, Y.S.L., N.H., Y.R., S.H.Y.; Roles/Writing - original draft, Y.S.L., N.H., Y.R., S.H.Y.; Writing – review & editing, all authors.

Financial support

Conflict of interest

S.H.Y. joined the MEDICAL IP, Co. Ltd. as a chief medical officer since November 2020. J.N.W. is an employer and machine learning researcher of MEDICAL IP, Co. Ltd. Other authors have no conflicts of interest to declare.

Acknowledgement

Appendix A. Supplementary data

Supplementary data to this article can be found online at https://doi.org/10.1016/j.clnu.2021.06.025.

References

[1] Cruz-Jentoft AJ, Sayer AA. Sarcopenia. Lancet 2019;393:2636–46.

[2] Cruz-Jentoft AJ, Bahat G, Bauer J, Boirie Y, Bruyere O, Cederholm T, et al. Sarcopenia: revised European consensus on definition and diagnosis. Age Ageing 2019;48:16–31.

[3] Prado CM, Heymsfield SB. Lean tissue imaging: a new era for nutritional assessment and intervention. JPEN - J Parenter Enter Nutr 2014;38:940–53.

[4] Buckinx F, Landi F, Cesari M, Fielding RA, Visser M, Engelke K, et al. Pitfalls in the measurement of muscle mass: a need for a reference standard. J Cachexia Sarcopenia Muscle 2018;9:269–78.

[5] Mitsiopoulos N, Baumgartner RN, Heymsfield SB, Lyons W, Gallagher D, Ross R. Cadaver validation of skeletal muscle measurement by magnetic resonance imaging and computerized tomography. J Appl Physiol 1985;1998(85):115–22.

[6] Shen W, Punyanitya M, Wang Z, Gallagher D, St-Onge MP, Albu J, et al. Total body skeletal muscle and adipose tissue volumes: estimation from a single abdominal cross-sectional image. J Appl Physiol 1985;2004(97):2333–8.

[7] Mourtzakis M, Prado CM, Lieffers JR, Reiman T, McCargar LJ, Baracos VE. A practical and precise approach to quantification of body composition in cancer patients using computed tomography images acquired during routine care. Appl Physiol Nutr Metabol 2008;33:997–1006.

[8] Shen W, Punyanitya M, Wang ZM, Gallagher D, St-Onge MP, Albu J, et al. Visceral adipose tissue: relations between single-slice areas and total volume. Am J Clin Nutr 2004;80:271–8.

[9] Boutin RD, Yao L, Canter RJ, Lenchik L. Sarcopenia: current concepts and imaging implications. Am J Roentgenol 2015;205:W255–66.

[10] Baracos VE, Arribas L. Sarcopenic obesity: hidden muscle wasting and its impact for survival and complications of cancer therapy. Ann Oncol 2018;29:1–9.

[11] Weston AD, Korfiatis P, Kline TL, Philbrick KA, Kostandy P, Sakinis T, et al. Automated abdominal segmentation of CT scans for body composition analysis using deep learning. Radiology 2019;290:669–79.

[12] Nowak S, Faron A, Luetkens JA, Geissler HL, Praktiknjo M, Block W, et al. Fully automated segmentation of connective tissue compartments for CT-based body composition analysis: a deep learning approach. Invest Radiol 2020;55:357–66.

[13] von Schulthess GK, Steinert HC, Hany TF. Integrated PET/CT: current applications and future directions. Radiology 2006;238:405–22.

[14] Poeppel TD, Krause BJ, Heusner TA, Boy C, Bockisch A, Antoch G. PET/CT for the staging and follow-up of patients with malignancies. Eur J Radiol 2009;70:382–92.

[15] Martin L, Birdsell L, Macdonald N, Reiman T, Clandinin MT, McCargar LJ, et al. Cancer cachexia in the age of obesity: skeletal muscle depletion is a powerful prognostic factor, independent of body mass index. J Clin Oncol 2013;31:1539–47.

[16] Shachar SS, Williams GR, Muss HB, Nishijima TF. Prognostic value of sarcopenia in adults with solid tumours: a meta-analysis and systematic review. Eur J Cancer 2016;57:58–67.

[17] Lee EY, Kim HC, Rhee Y, Youm Y, Kim KM, Lee JM, et al. The Korean urban rural elderly cohort study: study design and protocol. BMC Geriatr 2014;14:33.

[18] Hung CS, Lee JK, Yang CY, Hsieh HR, Ma WY, Lin MS, et al. Measurement of visceral fat: should we include retroperitoneal fat? PloS One 2014;9:e112355.

[19] Ronneberger O, Fischer P, Brox T. U-net: convolutional networks for biomedical image segmentation. Cham: Springer International Publishing; 2015. p. 234–41.

[20] Çiçek Ö, Abdulkadir A, Lienkamp SS, Brox T, Ronneberger O. 3D U-Net: learning dense volumetric segmentation from sparse annotation. Cham: Springer International Publishing; 2016. p. 424–32.

[21] Ioffe S, Szegedy C. Batch normalization: accelerating deep network training by reducing internal covariate shift. arXiv preprint arXiv:150203167. 2015.

[22] Krizhevsky A, Sutskever I, Hinton GE. Imagenet classification with deep convolutional neural networks. Adv Neural Inf Process Syst 2012:1097–105.

[23] He K, Zhang X, Ren S, Sun J. Delving deep into rectifiers: surpassing human-level performance on imagenet classification. Proc IEEE Int Conf Computer Vision 2015:1026–34.

[24] Hong N, Kim KJ, Lee SJ, Kim CO, Kim HC, Rhee Y, et al. Cohort profile: Korean Urban Rural Elderly (KURE) study, a prospective cohort on ageing and health in Korea. BMJ Open 2019;9:e031018.

[25] Song BM, Rhee Y, Kim CO, Youm Y, Kim KM, Lee EY, et al. Urban-rural differences explain the association between serum 25-hydroxyvitamin D level and insulin resistance in Korea. Nutrients 2014;6:5806–18.

[26] Song BM, Kim HC, Rhee Y, Youm Y, Kim CO. Association between serum 25-hydroxyvitamin D concentrations and depressive symptoms in an older Korean population: a cross-sectional study. J Affect Disord 2016;189:357–64.

[27] Lee EY, Lee SJ, Kim KM, Yun YM, Song BM, Kim JE, et al. Association of metabolic syndrome and 25-hydroxyvitamin D with cognitive impairment among elderly Koreans. Geriatr Gerontol Int 2017;17:1069–75.

[28] Hong N, Kim CO, Youm Y, Choi JY, Kim HC, Rhee Y. Dysmobility syndrome is associated with prevalent morphometric vertebral fracture in older adults: the Korean Urban-Rural Elderly (KURE) study. Arch Osteoporos 2018;13:86.

[29] Choi H, Kim HC, Song BM, Park JH, Lee JM, Yoon DL, et al. Serum uric acid concentration and metabolic syndrome among elderly Koreans: the Korean Urban Rural Elderly (KURE) study. Arch Gerontol Geriatr 2016;64:51–8.

[30] Choi H, Kim HC, Stefani KM, Lee JM, Yoon YM, Lee EY, et al. Serum high-density lipoprotein cholesterol concentration and functional state: the Korean Urban Rural Elderly (KURE) Study. Arch Gerontol Geriatr 2017;71:115–21.

[31] Chen LK, Woo J, Assantachai P, Auyeung TW, Chou MY, Iijima K, et al. Asian working group for sarcopenia: 2019 consensus update on sarcopenia diagnosis and treatment. J Am Med Dir Assoc 2020;21:300–7. e2.

[32] Engelke K, Adams JE, Armbrecht G, Augat P, Bogado CE, Bouxsein ML, et al. Clinical use of quantitative computed tomography and peripheral quantitative computed tomography in the management of osteoporosis in adults: the 2007 ISCD Official Positions. J Clin Densitom 2008;11:123–62.

[33] Hong N, Kim CO, Youm Y, Kim HC, Rhee Y. Low peak jump power is associated with elevated odds of dysmobility syndrome in community-dwelling elderly individuals: the Korean Urban Rural Elderly (KURE) study. Osteoporos Int 2018;29:1427–36.

[34] Binkley N, Krueger D, Buehring B. What's in a name revisited: should osteoporosis and sarcopenia be considered components of "dysmobility syndrome? Osteoporos Int 2013;24:2955–9.

[35] Taha AA, Hanbury A. Metrics for evaluating 3D medical image segmentation: analysis, selection, and tool. BMC Med Imag 2015;15:29.

[36] Ross R, Neeland IJ, Yamashita S, Shai I, Seidell J, Magni P, et al. Waist circumference as a vital sign in clinical practice: a consensus statement from the IAS and ICCR working group on visceral obesity. Nat Rev Endocrinol 2020;16:177–89.

[37] Chakraverty R, Pynsent P, Isaacs K. Which spinal levels are identified by palpation of the iliac crests and the posterior superior iliac spines? J Anat 2007;210:232–6.

[38] Chen LK, Liu LK, Woo J, Assantachai P, Auyeung TW, Bahyah KS, et al. Sarcopenia in Asia: consensus report of the Asian working group for sarcopenia. J Am Med Dir Assoc 2014;15:95–101.

[39] DeLong ER, DeLong DM, Clarke-Pearson DL. Comparing the areas under two or more correlated receiver operating characteristic curves: a nonparametric approach. Biometrics 1988;44:837–45.

[40] Davidson A. CT equipment market: made in China...and the USA. 2018.

[41] Sayer AA, Syddall H, Martin H, Patel H, Baylis D, Cooper C. The developmental origins of sarcopenia. J Nutr Health Aging 2008;12:427–32.

[42] Wang B, Torriani M. Artificial intelligence in the evaluation of body composition. Semin Muscoskel Radiol 2020;24:30–7.

[43] Mansoor A, Bagci U, Foster B, Xu Z, Papadakis GZ, Folio LR, et al. Segmentation and image analysis of abnormal lungs at CT: current approaches, challenges, and future trends. Radiographics 2015;35:1056–76.

[44] Iannessi A, Beaumont H, Hebert C, Dittlot C, Falewee MN. Computer tomography-based body surface area evaluation for drug dosage: quantitative radiology versus anthropomorphic evaluation. PloS One 2018;13:e0192124.

[45] Heymsfield SB, Martin-Nguyen A, Fong TM, Gallagher D, Pietrobelli A. Body circumferences: clinical implications emerging from a new geometric model. Nutr Metab 2008;5:24.

[46] Villa C, Primeau C, Hesse U, Hougen HP, Lynnerup N, Hesse B. Body surface area determined by whole-body CT scanning: need for new formulae? Clin Physiol Funct Imag 2017;37:183–93.